MATERIALS CHEMISTRY FRONTIERS

RESEARCH ARTICLE

View Article Online
View Journal | View Issue

Check for updates

Cite this: *Mater. Chem. Front.*, 2021, **5**, 4963

Electrochemical fixation of CO_2 over a Mo plate to prepare a Mo_2C film for electrocatalytic hydrogen evolution†

Hansheng Xiao,[a] Hua Zhu,[a] Wei Weng,[a] Kongzhai Li, *[b] Wei Li*[c] and Wei Xiao *[ad]

Received 20th March 2021,
Accepted 1st May 2021

DOI: 10.1039/d1qm00443c

rsc.li/frontiers-materials

Conversion of carbon dioxide into a hydrogen-evolution electrocatalyst is an ideal protocol to promote carbon neutrality by eliminating emissions of carbon dioxide and producing carbon-free hydrogen energy. Electrochemical fixation of carbon dioxide in molten salts by using a Mo-plate cathode and a Ni–Cr anode is herein demonstrated to produce a cathodic Mo_2C film and anodic oxygen. The molten salt electrochemical method offers an efficient modulation of thickness, adhesion and more importantly, interfacial confinement between the Mo_2C film and Mo. The resulting Mo_2C–Mo binder-free electrode hence shows enhanced electrocatalytic activity towards hydrogen evolution, as rationalized by the lower hydrogen adsorption energy at the Mo_2C–Mo interface. The electrochemical reduction of carbon dioxide over a metal substrate is therefore a generic method integrating fixation of carbon dioxide and surface carbonization of a metal to functional films.

Published on 07 May 2021. Downloaded on 5/20/2025 7:35:14 PM.

Introduction

Carbon neutrality has become a worldwide consensus.[1–5] For example, the Chinese government recently announced that nation-wide carbon neutrality must be achieved by the year 2060. Reducing carbon dioxide emissions and developing carbon-free clean energy are therefore in urgent need.[5,6]

Electrochemical conversion of CO_2 in molten salts to valuable chemicals is an emerging technology, which is capable of using intermittent renewable energy and achieving efficient CO_2 fixation.[6–10] The solubility of CO_2 in molten salts is several orders of magnitude higher than that in aqueous electrolytes, enabling a high-throughput capture and conversion process.[9–11] Moreover, the chemical reactions could proceed much easier in molten salt due to superior reaction kinetics in high-temperature molten salts compared to room-temperature media.[8] However, in molten salts, CO_2 is mainly electrochemically converted to carbonaceous materials, whose functionality needs to be substantially improved.[9]

Another route for curbing the greenhouse effect is to develop sustainable carbon-free clean energy to supplement fossil fuels.[12–15] Electrolytic production of hydrogen using solar/wind electricity as energy sources is one of the promising alternatives due to the high-energy density, carbon-free characteristics, and resource abundance of hydrogen.[12–15] However, the application of electrolytic hydrogen energy relies on the development of noble-metal-free catalysts for the hydrogen evolution reaction (HER).[16–18,37,41] Molybdenum carbides are promising candidates as HER catalysts due to the platinum-like d-band electronic structure.[19–22,38–40] The preparation of molybdenum carbides based on thermal combination between Mo and carbon is challenged by inadequate modulation of the microstructure of the Mo–C, with the HER activity being yet to be exploited.[23–26] Besides, the prepared powdery catalysts are commonly immobilized onto conductive substrates using organic binders. This electrode configuration tends to increase resistance and block active sites, causing performance degradation.[24,27,28] Such catalyst powders probably fall off from the substrate due to the hydrogen-evolution-induced turbulence on the electrode–electrolyte interface, particularly in industrial applications with a high current density. *In situ* growth of a binder-free Mo_2C film on conductive substrates is an effective way to mitigate the above problems.[29]

Herein, a Mo_2C film is *in situ* generated from the metallic Mo substrate during electrochemical splitting of CO_2 in molten

[a] *School of Resource and Environmental Sciences, Hubei International Scientific and Technological Cooperation Base of Sustainable Resource and Energy, Wuhan University, Wuhan 430072, P. R. China. E-mail: 00030042@whu.edu.cn*
[b] *State Key Laboratory of Complex Nonferrous Metal Resources Clean Utilization Engineering, Faculty of Chemical Engineering, Kunming University of Science and Technology, Kunming 650093, P. R. China. E-mail: kongzhai.li@foxmail.com*
[c] *Institute of Rare Metals, Guangdong Academy of Sciences, Guangzhou 510650, P. R. China. E-mail: shs9320@163.com*
[d] *College of Chemistry and Molecular Sciences, Hubei Key Laboratory of Electrochemical Power Sources, Wuhan University, Wuhan 430072, P. R. China*
† Electronic supplementary information (ESI) available: More characterizations. See DOI: 10.1039/d1qm00443c

Published on 07 May 2021. Downloaded on 5/20/2025 7:35:14 PM.

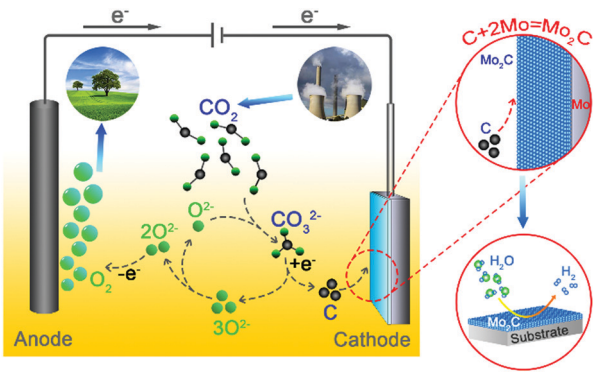

Fig. 1 Schematic illustration on electrochemical fixation of CO_2 in molten salts over a Mo substrate to prepare functional Mo–C films.

salts. As illustrated in Fig. 1, gaseous CO_2 is firstly captured by O^{2-} in molten carbonate salts to generate soluble CO_3^{2-},[6,9,10,30] which is then electro-reduced to carbon on the metallic Mo plate cathode ($CO_3^{2-} + 4e^- = C + 3O^{2-}$). The deposited carbon particles simultaneously react with the Mo substrate, resulting in the *in situ* growth of a surface Mo_2C film ($C + 2Mo = Mo_2C$, and $\Delta G^\theta = -56.378$ kJ mol^{-1} at 900 °C).[29,31–34] Correspondingly, deposition of carbon from electroreduction of CO_3^{2-} is accompanied by the release of O^{2-}, which then diffuses to the inert anode to be discharged as O_2 ($2O^{2-} - 4e^- = O_2$).[6,9,10] As a result, CO_2 is electrochemically split to facilitate the *in situ* growth of a Mo_2C film on the metallic Mo cathode, with O_2 being released on the inert anode simultaneously. The as-prepared structure possesses the merits of being free of binder, strong adhesion and well-defined interface, endowing the Mo_2C layer with enhanced electrocatalytic activity toward the HER and long-term stability.[24] The interfacial confinement between Mo_2C and Mo is rationalized based on density-functional theory (DFT) simulations. This strategy of electrochemical fixation of CO_2 over a metallic substrate to prepare functional films of metal carbides is also extended to prepare other films of metal carbides.

Experimental

Synthesis of catalyst

Pure Li_2CO_3 (98% purity, Sinopharm Chemical Reagent Co. Ltd), 300 g, was weighed and used as the electrolyte, which was filled into an alumina crucible (80 mm in diameter, and 150 mm in length) and then put in a vertical tubular reactor. The salt was kept at 400 °C for more than 24 h to remove the moisture and then heated up to 900 °C at the rate of 5 °C min^{-1} under the protection of a high-purity argon (Wuhan Huaerwen Industrial Co. Ltd) gas atmosphere. A Mo plate (14 mm × 14 mm × 0.2 mm) was polished using silicon carbide papers with different grit sizes to make it smooth, then washed with deionized water and alcohol, and finally dried at 60 °C in an oven. After that, using Ni–Cr alloy (20 wt% Cr, 80 wt% Ni, and 1 mm in diameter, Taizhou Xinai electrothermal alloy material Co. Ltd) as an inert anode and a Ni plate as a cathode, pre-electrolysis was conducted at a constant cell voltage of 1.6 V for 8 h to remove impurities and residual moisture. Afterwards the cathode was changed to the polished Mo plate and constant-voltage electrolysis was carried out at 3.1 V for different times to obtain the Mo_2C-coated Mo plate, with high-purity CO_2 being injected into the molten salts at 50 mL min^{-1} during the whole process. After electrolysis, the Mo plate cathode was lifted out from the molten salt and cooled to room temperature. Finally, the Mo_2C-coated Mo plate (denoted as Mo_2C/Mo-*t*, in which *t* means the electrolysis time in minute) was obtained after thoroughly washing with deionized water and alcohol to remove the excess salt. For example, Mo_2C/Mo-60 means the sample obtained at 3.1 V for 60 minutes. To investigate the versatility of the method, the electrochemical treatment of a tungsten substrate was also conducted at 3.1 V for 2 h at 900 °C in molten Li_2CO_3.

Characterization

Phase compositions of the electrode surfaces were measured by using X-ray diffraction (XRD) patterns on a Rigaku Miniflex600 instrument at 40 kV and 15 mA with Cu Kα radiation, and the diffraction data in the 2θ range from 5° to 90° were analysed at a scan rate of 5° min^{-1}. The morphology and elemental distribution were obtained by using scanning electron microscopy (a Tescan Mira3 SEM equipped with an energy dispersive X-ray spectroscopy instrument (EDS, Oxford Instruments X-Max 20)) at an accelerating voltage of 20.0 kV and working distance of 15.05 mm. X-Ray photoelectron spectroscopy (XPS) was performed on a Thermo Fisher Scientific ESCALAB250Xi spectrometer with a monochromatic Al Kα X-ray source. The recorded XPS spectra were calibrated according to the C 1s peak at 284.8 eV. The tail gases from the reactor were measured using a gas chromatograph (Shimadzu, GC-2014) equipped with a flame ionization detector (FID) and a thermal conductivity detector (TCD).

Electrochemical measurements

The electrochemical performance values for the HER tests were collected on a multichannel electrochemical workstation (Solartron Analytical 1470E) using a three-electrode system in 0.5 M H_2SO_4 solution. The obtained Mo_2C-coated Mo plate (0.5 × 0.5 cm^2) served as the working electrode, with a KCl-saturated Ag/AgCl electrode (Tianjin Aida Hengsheng Technology Development Co. Ltd) and a graphitic rod (10 mm in diameter, Dongguan Zehui New Material Technology Co. Ltd) as the reference electrode and counter electrode. All the obtained potentials were calibrated to a reversible hydrogen electrode (RHE) according to the formula $E_{RHE} = E_{Ag/AgCl} + 0.059\ V \times pH + 0.1989\ V$. For comparison, a bare Mo plate was also measured. The commercial Pt/C (20 wt% Pt, Sigma-Aldrich) catalyst loaded on the polished Mo plate (the Pt loading was 0.4 mg cm^{-2}) was also tested for the HER. All the HER data were obtained by linear sweep voltammetry (LSV) at a scanning rate of 5 mV s^{-1}. Electrochemical impedance spectra (EIS) were obtained at 0.15 V (*vs.* RHE) between 100 kHz and 0.01 Hz with an AC (alternating current) potential amplitude of 5 mV. All the LSV polarization curves, referring to previous work,[35] were obtained by resistance compensation (*iR*) (85%) using the internal

 This journal is © The Royal Society of Chemistry and the Chinese Chemical Society 2021

Published on 07 May 2021. Downloaded on 5/20/2025 7:35:14 PM.

resistance (R_s) obtained from the EIS plots. The catalyst durability test was assessed by cyclic voltammetry (CV) at a scanning rate of 100 mV s^{-1} for 1000 cycles. The electrochemical surface areas (ECSAs) of the samples were estimated by using capacitance (C_{dl}) according to the CV curves at scanning rates from 10 to 50 mV s^{-1}. Turnover frequency (TOF) is estimated from the pseudo-capacitance of the Mo-based catalysts and obtained using eqn (1):

$$\mathrm{TOF} = (J \times A)/(n \times F \times m) \quad (1)$$

where J (A cm^{-2}) is the current density at a specific potential, A (cm^2) is the surface area of the electrode (0.196 cm^2), n is the number of electrons transferred per molecule, 2 for the HER, F is Faraday's constant (96 485 C mol^{-1}), and m is the number of Mo atoms in Mo_2C by weighing the mass of Mo sheet before and after the reaction.

Theoretical calculations

The HER process on Mo (110), Mo_2C (121) and Mo (110)–Mo_2C (121) was investigated by the Vienna *ab-initio* simulation package (VASP). The revised Perdew–Burke–Ernzerhof (RPBE) of the generalized gradient approximation (GGA) was used to calculate the hydrogen adsorption energy. The PAW pseudo-potential was used to describe the interaction between valence electrons and ions. Four Mo layers and four Mo–C layers were used to simulate the Mo (110) and Mo_2C (121) surfaces, respectively. The energy convergence of 1.0×10^{-5} eV and the cut-off energy of 400 eV at the gamma point were adopted in the geometry optimization. Gibbs free energy changes (ΔG) were calculated by the standard hydrogen electrode (SHE) model at U = 0 V *vs.* SHE at pH = 0. After geometry optimization, the projected density of states (PDOS) plots of active sites in Mo (110), Mo_2C (121) and Mo (110)–Mo_2C (121) were calculated with the energy convergence of 1×10^{-5} eV and the Monkhorst–Pack mesh of 2 × 2 × 1.

Results and discussion

Surface carbonization of the Mo plate cathode is realized by electrolysis of CO_2 over a Mo cathode at 3.1 V in Li_2CO_3 molten salt at 900 °C. The bare Mo plate shows a smooth surface (Fig. 2a). After electrolysis for 60 minutes, spherical particles appear, showing a highly interconnected configuration between adjacent particles (Fig. 2b). Formation of a film is also revealed by the apparent colour change of the Mo plate surface after electrolysis (Fig. 2c). The details of the layer are further revealed by the cross-sectional analysis. Compared to the bare Mo plate (Fig. 2d), an outer layer closely attached to the Mo substrate was obviously observed (Fig. 2e), with a thickness of ~4 μm. Fig. S1 (ESI†) shows the boundary between the (110) plane of Mo and (100) plane of Mo_2C. The elemental distribution of the molybdenum plate after electrolysis was further investigated by EDS linear sweep analysis (Fig. 2f). The corresponding mappings are listed in Fig. 2g–i. The results demonstrate the homogeneous distribution of Mo and C in the surface layer and also indicate the interface between the film and substrate. A good adhesion exists between the Mo_2C film and Mo substrate, as reflected by the robustness

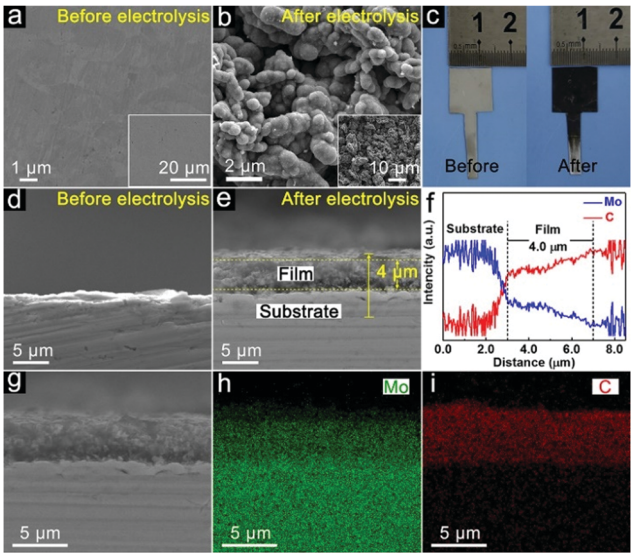

Fig. 2 Typical SEM images for the surfaces of the Mo plate (a) and obtained Mo_2C/Mo-60 (b). (c) Digital photos of Mo plates before and after electrolysis. Cross-sectional SEM images of Mo (d) and Mo_2C/Mo-60 (e). Corresponding EDS results of linear sweep analysis (f) and elemental distribution mappings (g–i) for Mo_2C/Mo-60.

of the film even upon rigorous rinsing or ultrasonication in water. Such a stable integration originates from the strong Mo–C bond in the interface, which is important to HER applications, especially in high-current operations.

The phase and surface compositions were characterized by XRD and XPS. As presented in the XRD results (Fig. 3a), the additional diffraction peaks for Mo_2C (JCPDS No. 65-8766) can be detected after electrolysis in molten salt. The existence of Mo_2C is also confirmed by the fitting of the Mo–C XPS peaks in the C 1s and Mo 3d regions (Fig. 3c and d). The Mo 3d XPS spectrum also presents the peaks of Mo^{6+} and Mo^{4+}, originating from inevitable oxidation when exposed to air.[36] Mo^{6+} and Mo^{4+} species were proved to be inactive for the HER, while Mo^{2+} species were believed to be the active centers for electrocatalytic HER, which is reported in previous studies.[42] The generation of

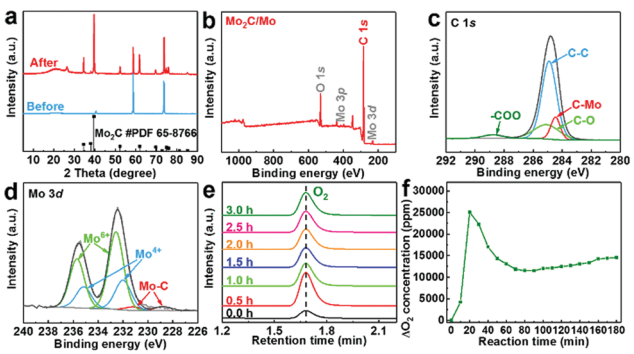

Fig. 3 (a) XRD patterns of Mo_2C/Mo-60 and Mo film. (b) XPS survey spectrum of the Mo_2C/Mo-60. High-resolution C 1s (c) and Mo 3d (d) XPS spectra for Mo_2C/Mo-60. (e) Gas chromatogram of oxygen flowing out from the experimental system at different times. (f) Variation of oxygen concentration during electrolysis at 3.1 V.

Published on 07 May 2021. Downloaded on 5/20/2025 7:35:14 PM.

cathodic Mo_2C is accompanied by anodic oxygen evolution, as revealed by the sharp increase in oxygen concentration upon electrolysis (Fig. 3e and f). Thus, electrochemical splitting of CO_2 in molten salts results in cathodic Mo_2C films over the Mo cathode and anodic oxygen.

The thickness of the Mo_2C layer is dependent on the electrolysis time. A 10 minute electrolysis generates a thin Mo_2C layer being only 0.7 μm (Fig. 4a), which increases to 5.8 μm after prolonging the electrolysis time to 120 minutes (Fig. 4b). Extending the electrolysis time offers a stronger penetration of electrodeposited carbon into Mo, facilitating a deeper Mo-to-Mo_2C conversion (Fig. 4c). There is a linear relationship between the square of thickness and the electrolysis time (not shown), and the correlation coefficient is higher than 0.99. Such a linear correlation between the square of thickness and the electrolysis time indicates that the generation of Mo–C film is governed by diffusion.

Too short an electrolysis time leads to insufficient surface coverage of the Mo plate by active Mo_2C, while excessively prolonged electrolysis induces a thick Mo_2C layer, causing increased electrical resistance between the Mo substrate and reaction interface. Electrolysis time also affects the morphology of the generated Mo_2C particles. Electrolysis for a short time results in a loosened structure in the Mo_2C layer (10 min. in Fig. 4d and 30 min. in Fig. 4e), with the inner substrate being partially exposed due to the insufficient coverage. Prolonging the electrolysis time results in partial sintering and coalescence between adjacent particles, generating less-porous structures (60 min. in Fig. 2b and 120 min. in Fig. 4f, and also illustrated in Fig. 4g). Mo_2C particles are interconnected, but still maintain partial independence and relative isolation with obvious outlines of every single Mo_2C particle (Fig. 2b and Fig. 4f). Such a special integration in coalescence and independence between Mo_2C particles of dense structure contributes to the exposure of active sites, electron-transfer and stability, indicating the appealing performance as a HER electrocatalyst.

As a generic protocol, electrochemical fixation of CO_2 on a metallic substrate to prepare a metal-carbide film is extended to generate tungsten carbide. As shown in Fig. S2 (ESI†), molten salt electrolysis of CO_2 in molten salts over the tungsten substrate results in WC films over the W substrate. The generation of metal (Mo or W) carbides is *via* combination of electrodeposited carbon and metal substrates. The generation of Mo–C and W–C *via* combination is thermodynamically spontaneous at 900 °C. In contrast, formation of Fe–C *via* combination is thermodynamically uphill. Hence, the protocol can be used to generate Mo–C and W–C, but can hardly be used to generate Fe–C. The attempt at using Fe as a cathode appears to have failed in terms of preparation of Fe–C films over an Fe substrate, under similar experimental conditions.

The electrocatalytic performance of the Mo_2C/Mo plates for the HER was tested by recording polarization curves in a three-electrode system in 0.5 M H_2SO_4 solution, using bare Mo plate and commercial Pt/C for comparison. As shown in Fig. 5a, the bare Mo plate exhibits a relatively low electrocatalytic activity for the HER, and needs an overpotential of 375 mV to provide 10 mA cm^{-2}. The overpotential is only 149 mV at 10 mA cm^{-2} for the Mo_2C/Mo-60 obtained by electrolysis at 3.1 V for 60 minutes. The Mo_2C/Mo-60 presents the lowest overpotential (Fig. 5b) and the highest electrochemically active surface area (Fig. 5c and Fig. S3 (ESI†), as suggested by the largest value of C_{dl}), as well as the highest turnover frequency (Fig. S4, ESI†), implying that the optimized electrolysis time is 60 minutes for Mo_2C-coated Mo plates. Correspondingly, the optimized thickness of the Mo_2C layer obtained after 60 minutes is 4 μm, as shown in Fig. 4c. The optimized sample of Mo_2C/Mo-60 also presents a much lower Tafel slope (77.89 mV dec^{-1}) than that for bare Mo (321.64 mV dec^{-1}), as shown in Fig. 5d. The enhanced activity originates from much lower charge transfer resistance of Mo_2C/Mo-60 than that of the bare Mo, as revealed by the smaller

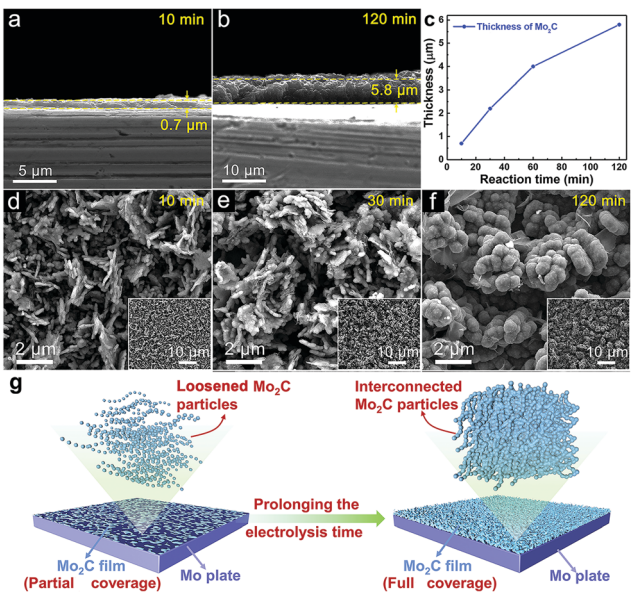

Fig. 4 Cross-sectional SEM images of Mo_2C/Mo-10 (a) and Mo_2C/Mo-120 (b). (c) Thickness change of the Mo_2C layer *vs.* electrolysis time. SEM images of Mo_2C/Mo-10 (d), Mo_2C/Mo-30 (e) and Mo_2C/Mo-120 (f). (g) Illustration of the changes of thickness and morphology of the Mo_2C film by prolonging the electrolysis time.

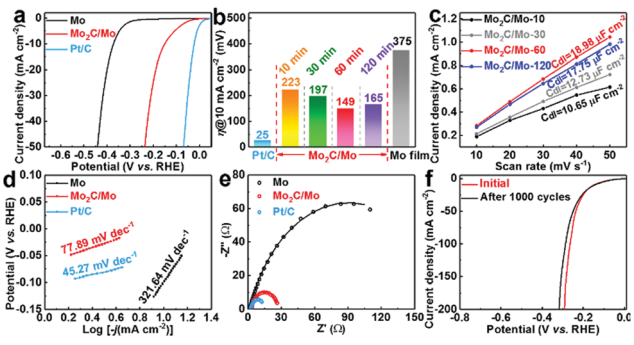

Fig. 5 (a) Polarization curves of the prepared Mo_2C/Mo-60, bare Mo plate and Pt/C catalysts at 5 mV s^{-1} in 0.5 M H_2SO_4 at 25 °C. (b) Overpotentials at 10 mA cm^{-2}. (c) Linear relationship between the capacitance current density and scan rate. (d) Corresponding Tafel plots and (e) EIS Nyquist plots of different samples. (f) Polarization curves of Mo_2C/Mo-60 before and after 1000 cycles.

 This journal is © The Royal Society of Chemistry and the Chinese Chemical Society 2021

Published on 07 May 2021. Downloaded on 5/20/2025 7:35:14 PM.

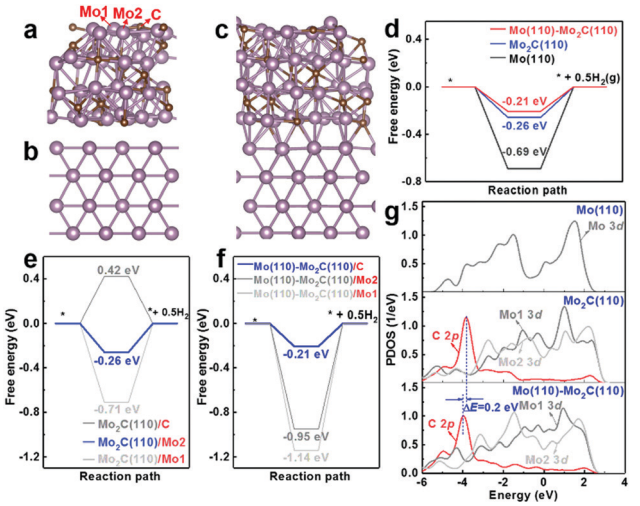

Fig. 6 (a–c) Optimized geometry structures of (a) Mo_2C (121), (b) Mo (110), and (c) Mo (110)–Mo_2C (121). (d) The calculated energy profiles for the HER on Mo (110), Mo_2C (121), and Mo (110)–Mo_2C (121). (e) The calculated energy profiles for the HER on different reaction sites of Mo_2C (121): the reaction sites of C, Mo1, and Mo2 are denoted as Mo_2C (121)/C, Mo_2C (121)/Mo1, and Mo_2C (121)/Mo2, respectively. (f) The calculated energy profiles for the HER on different surface catalytic sites of M o(110)–Mo_2C (121): the reaction sites of C, Mo1, and Mo2 are denoted as Mo (110)–Mo_2C (121)/C, Mo (110)–Mo_2C (121)/Mo1, and Mo (110)–Mo_2C (121)/Mo2, respectively. (g) Projected density of states (PDOS) plots of surface catalytic sites in Mo (110), Mo_2C (121), and Mo (110)–Mo_2C (121).

semicircle diameter (Fig. 5e and Table S1, ESI†). The Mo_2C layer consists of highly interconnected particles, resulting in both efficient electron-transfer networks and full exposure of active sites. The Mo_2C/Mo-60 also shows appealing long-term stability, as evidenced by the neglectable change of the LSV curve after 1000 cycles (Fig. 5f). After the stability test, the SEM images and XRD patterns of the products hardly changed (Fig. S5, ESI†). Such a superior stability is attributed to the strong adherence of the Mo_2C layer to the substrate because of its *in situ* generation from the substrate in molten salts. The performance of the obtained Mo_2C-coated Mo plate is comparable with or superior to that of the recently reported Mo_2C-based catalysts for the HER in acid solutions (Table S2, ESI†).

In addition to the strong adhesion of Mo_2C film to the Mo substrate and well-defined microstructure of interconnected Mo_2C particles, another factor contributing to the enhanced activity of Mo_2C/Mo is the synergic effect between the Mo substrate and Mo_2C film, as revealed by DFT calculations (Fig. 6). Fig. 6a–c present the optimized structures of Mo_2C (121), Mo (110), and Mo (110)–Mo_2C (121), respectively, with the proton-adsorbed structures presented in Fig. S6 (ESI†).

As shown in Fig. 6d, the Mo (110)–Mo_2C (121) surface possesses a lower free energy (−0.21 eV) for the HER than that of both the Mo_2C (121) surface (−0.26 eV) and Mo (110) surface (−0.69 eV). This result suggests that the synergy between Mo_2C and Mo is beneficial to the enhancement of the HER activity. The activity enhancement is attributed to the transformation of active sites of the Mo (110)–Mo_2C (121) heterostructure for hydrogen adsorption. Both the Mo_2C (121) and Mo (110)–Mo_2C (121) surfaces contain three kinds of surface catalytic sites (C, Mo1 and Mo2, see Fig. 6a), while the Mo (110) surface contains only one catalytic site (the Mo atom site). The preferential catalytic site for hydrogen adsorption is the Mo2 site on the Mo_2C (121) surface, as revealed by the lowest free energy of Mo_2C (121)/Mo2 in Fig. 6e. However, the lowest free energy for the HER transforms to the C site on the Mo (110)–Mo_2C (121) surfaces, denoted as Mo (110)–Mo_2C (121)/C in Fig. 6f. Therefore, the main active site for the HER changes from the Mo2 site on Mo_2C (121) to the C site on the Mo (110)–Mo_2C (121) heterostructure. The higher HER activity of the C site on the Mo (110)–Mo_2C (121) surface is also manifested by the PDOS files (Fig. 6g), which show that the C 2p state of the Mo (110)–Mo_2C (121) heterostructure is located in the more negative region compared to the electronic states of other surface sites. The higher reducing state of the C site on Mo (110)–Mo_2C (121) hence facilitates reduction of protons and results in enhanced activity towards the HER.

Conclusions

In summary, electrochemical fixation of carbon dioxide in molten salts is demonstrated as an efficient surface carbonization method of metallic substrates. This electrochemical route couples value-added conversion of CO_2 with fabrication of advanced materials, contributing to upgraded utilization of CO_2. The resulting Mo_2C film *in situ* generated from the Mo plate substrate upon CO_2 fixation shows a good adhesion with the substrate and well-defined microstructure. The strong synergic effect between the Mo_2C film and the Mo substrate contributes to lower free energy for the adsorption of protons. When tested as the electrocatalyst for the HER, the optimized Mo_2C-coated Mo plate presents enhanced performance. The strategy herein provides a generic protocol for curbing the greenhouse effect by facilely converting carbon dioxide into functional films for renewable energy applications.

Author contributions

H. Xiao and W. Weng performed the molten salt electrolysis experiments, material characterizations, and HER tests, as well as wrote the draft manuscript. W. Li and K. Li performed the DFT calculations. W. Xiao and H. Zhu conceived the idea, analyzed the data, and revised the manuscript. All authors discussed the results and commented on the manuscript.

Conflicts of interest

The authors declare that they have no known competing financial interests or personal relationships that could have appeared to influence the work reported in this paper.

Acknowledgements

The authors acknowledge the funding support from the National Natural Science Foundation of China (51722404, 51804221, and 91845113), the National Key R&D Program of

Published on 07 May 2021. Downloaded on 5/20/2025 7:35:14 PM.

China (2018YFE0201703), the China Postdoctoral Science Foundation (2018M642906 and 2019T120684), and the Hubei Provincial Natural Science Foundation of China (2019CFA065).

References

1 S. Popovic, M. Smiljanic, P. Jovanovic, J. Vavra, R. Buonsanti and N. Hodnik, Stability and degradation mechanisms of copper-based catalysts for electrochemical CO_2 reduction, *Angew. Chem., Int. Ed.*, 2020, **59**, 14736–14746.

2 L. Fan, C. Xia, F. Yang, J. Wang, H. Wang and Y. Lu, Strategies in catalysts and electrolyzer design for electrochemical CO_2 reduction toward C_{2+} products, *Sci. Adv.*, 2020, **6**, eaay3111.

3 Y. Liu, D. Tian, A. N. Biswas, Z. Xie, S. Hwang, J. H. Lee, H. Meng and J. G. Chen, Transition metal nitrides as promising catalyst supports for tuning CO/H_2 syngas production from electrochemical CO_2 reduction, *Angew. Chem., Int. Ed.*, 2020, **59**, 11345–11348.

4 T. Yuan, Z. Hu, Y. Zhao, J. Fang, J. Lv, Q. Zhang, Z. Zhuang, L. Gu and S. Hu, Two-dimensional amorphous SnO_x from liquid metal: mass production, phase transfer, and electrocatalytic CO_2 reduction toward formic acid, *Nano Lett.*, 2020, **20**, 2916–2922.

5 W. Weng, S. Wang, W. Xiao and X. W. Lou, Direct conversion of rice husks to nanostructured SiC/C for CO_2 photoreduction, *Adv. Mater.*, 2020, **32**, 2001560.

6 X. Liang, J. Xiao, W. Weng and W. Xiao, Electrochemical reduction of carbon dioxide and iron oxide in molten salts to Fe/Fe_3C modified carbon for electrocatalytic oxygen evolution, *Angew. Chem., Int. Ed.*, 2021, **60**, 2120–2124.

7 W. Weng, B. M. Jiang, Z. Wang and W. Xiao, In situ electrochemical conversion of CO_2 in molten salts to advanced energy materials with reduced carbon emissions, *Sci. Adv.*, 2020, **6**, eaay9278.

8 W. Weng, J. R. Yang, J. Zhou, D. Gu and W. Xiao, Template-free electrochemical formation of silicon nanotube from silica, *Adv. Sci.*, 2020, **7**, 2001492.

9 W. Weng, L. Tang and W. Xiao, Capture and electro-splitting of CO_2 in molten salts, *J. Energy Chem.*, 2019, **28**, 128–143.

10 T. Lv, J. Xiao, W. Weng and W. Xiao, Electrochemical fixation of carbon dioxide in molten salts on liquid zinc cathode to zinc@graphitic carbon spheres for enhanced energy storage, *Adv. Energy Mater.*, 2020, **10**, 2002241.

11 J. Yang, W. Weng and W. Xiao, Electrochemical synthesis of ammonia in molten salts, *J. Energy Chem.*, 2020, **43**, 195–207.

12 W. Weng, J. Zhou, D. Gu and W. Xiao, Thermoelectrochemical formation of Fe/Fe_3C@hollow N-doped carbon in molten salts for enhanced catalysis, *J. Mater. Chem. A*, 2020, **8**, 4800–4806.

13 J. Cai, Y. Song, Y. Zang, S. Niu, Y. Wu, Y. Xie, X. Zheng, Y. Liu, Y. Lin, X. Liu, G. Wang and Y. Qian, N-induced lattice contraction generally boosts the hydrogen evolution catalysis of P-rich metal phosphides, *Sci. Adv.*, 2020, **6**, eaaw8113.

14 J. Zhou, H. Xiao, W. Weng, D. Gu and W. Xiao, Interfacial confinement of $Ni\text{-}V_2O_3$ in molten salts for enhanced electrocatalytic hydrogen evolution, *J. Energy Chem.*, 2020, **50**, 280–285.

15 C. H. Chen, D. Wu, Z. Li, R. Zhang, C. G. Kuai, X. R. Zhao, C. K. Dong, S. Z. Qiao, H. Liu and X. W. Du, Ruthenium-based single-atom alloy with high electrocatalytic activity for hydrogen evolution, *Adv. Energy Mater.*, 2019, **9**, 1803913.

16 J. Ren, Z. Hu, C. Chen, Y. Liu and Z. Yuan, Integrated Ni_2P nanosheet arrays on three-dimensional Ni foam for highly efficient water reduction and oxidation, *J. Energy Chem.*, 2017, **26**, 1196–1202.

17 E. L. W. M. G. Walter, J. R. McKone, S. W. Boettcher, Q. Mi, E. A. Santori and N. S. Lewis, Solar water splitting cells, *Chem. Rev.*, 2016, **10**, 6446–6473.

18 Q. Lu, Y. Yu, Q. Ma, B. Chen and H. Zhang, 2D transition-metal-dichalcogenide-nanosheet-based composites for photocatalytic and electrocatalytic hydrogen evolution reactions, *Adv. Mater.*, 2016, **28**, 1917–1933.

19 Z. Wei, X. Hu, S. Ning, X. Kang and S. Chen, Supported heterostructured MoC/Mo_2C nanoribbons and nanoflowers as highly active electrocatalysts for hydrogen evolution reaction, *ACS Sustainable Chem. Eng.*, 2019, **7**, 8458–8465.

20 W. Yuan, Q. Huang, X. Yang, Z. Cui, S. Zhu, Z. Li, S. Du, N. Qiu and Y. Liang, Two-dimensional lamellar Mo_2C for electrochemical hydrogen production: insights into the origin of hydrogen evolution reaction activity in acidic and alkaline electrolytes, *ACS Appl. Mater. Interfaces*, 2018, **10**, 40500–40508.

21 W. Zheng, T. P. Cotter, P. Kaghazchi, T. Jacob, B. Frank, K. Schlichte, W. Zhang, D. S. Su, F. Schuth and R. Schlogl, Experimental and theoretical investigation of molybdenum carbide and nitride as catalysts for ammonia decomposition, *J. Am. Chem. Soc.*, 2013, **135**, 3458–3464.

22 C. Wan, Y. N. Regmi and B. M. Leonard, Multiple phases of molybdenum carbide as electrocatalysts for the hydrogen evolution reaction, *Angew. Chem., Int. Ed.*, 2014, **53**, 6407–6410.

23 L. Chai, L. Zhang, X. Wang, Z. Ma, T. T. Li, H. Li, Y. Hu, J. Qian and S. Huang, Construction of hierarchical Mo_2C nanoparticles onto hollow N-doped carbon polyhedrons for efficient hydrogen evolution reaction, *Electrochim. Acta*, 2019, **321**, 134680.

24 X. X. Liang, W. Weng, D. Gu and W. Xiao, Nickel based oxide film formed in molten salts for efficient electrocatalytic oxygen evolution, *J. Mater. Chem. A*, 2019, **7**, 10514–10522.

25 C. Lv, Z. Huang, Q. Yang and C. Zhang, Nanocomposite of MoO_2 and MoC loaded on porous carbon as an efficient electrocatalyst for hydrogen evolution reaction, *Inorg. Chem. Front.*, 2018, **5**, 446–453.

26 M. Y. Gao, C. Yang, Q. B. Zhang, J. R. Zeng, X. T. Li, Y. X. Hua, C. Y. Xu and P. Dong, Facile electrochemical preparation of self-supported porous Ni–Mo alloy microsphere films as efficient bifunctional electrocatalysts for water splitting, *J. Mater. Chem. A*, 2017, **5**, 5797–5805.

27 X. Yu, M. Wang, X. Gong, Z. Guo, Z. Wang and S. Jiao, Self-supporting porous CoP-based films with phase-separation structure for ultrastable overall water electrolysis at large current density, *Adv. Energy Mater.*, 2018, **8**, 1802445.

 This journal is © The Royal Society of Chemistry and the Chinese Chemical Society 2021

Published on 07 May 2021. Downloaded on 5/20/2025 7:35:14 PM.

28 Z. Wang, Y. Inoue, T. Hisatomi, R. Ishikawa, Q. Wang, T. Takata, S. Chen, N. Shibata, Y. Ikuhara and K. Domen, Overall water splitting by Ta_3N_5 nanorod single crystals grown on the edges of $KTaO_3$ particles, *Nat. Catal.*, 2018, **1**, 756–763.

29 M. Fan, H. Chen, Y. Wu, L. L. Feng, Y. Liu, G. D. Li and X. Zou, Growth of molybdenum carbide micro-islands on carbon cloth toward binder-free cathodes for efficient hydrogen evolution reaction, *J. Mater. Chem. A*, 2015, **3**, 16320–16326.

30 M. Johnson, J. Ren, M. Lefler, G. Licht, J. Vicini, X. Liu and S. Licht, Carbon nanotube wools made directly from CO_2 by molten electrolysis: value driven pathways to carbon dioxide greenhouse gas mitigation, *Mater. Today Energy*, 2017, **5**, 230–236.

31 Z. Zhang, Q. Song, B. Jiang, H. Xie, H. Yin, Z. Ning and Q. Xu, Electrochemically assisted carbonization of Nb in molten salt, *Surf. Coat. Technol.*, 2019, **358**, 865–872.

32 X. Zou, K. Zheng, X. Lu, Q. Xu and Z. Zhou, Solid oxide membrane-assisted controllable electrolytic fabrication of metal carbides in molten salt, *Faraday Discuss.*, 2016, **190**, 53–69.

33 X. Zou, L. Ji, X. Lu and Z. Zhou, Facile electrosynthesis of silicon carbide nanowires from silica/carbon precursors in molten salt, *Sci. Rep.*, 2017, **7**, 9978.

34 N. J. Siambun, H. Mohamed, D. Hu, D. Jewell, Y. K. Beng and G. Z. Chen, Utilisation of carbon dioxide for electro-carburisation of mild steel in molten carbonate salts, *J. Electrochem. Soc.*, 2011, **158**, H1117–H1124.

35 M. Ming, Y. Ma, Y. Zhang, L. B. Huang, L. Zhao, Y. Y. Chen, X. Zhang, G. Fan and J. S. Hu, 3D nanoporous Ni/V_2O_3 hybrid nanoplate assemblies for highly efficient electrochemical hydrogen evolution, *J. Mater. Chem. A*, 2018, **6**, 21452–21457.

36 L. Ji, J. Wang, L. Guo and Z. Chen, In situ O_2-emission assisted synthesis of molybdenum carbide nanomaterials as an efficient electrocatalyst for hydrogen production in both acidic and alkaline media, *J. Mater. Chem. A*, 2017, **5**, 5178–5186.

37 F. X. Ma, H. B. Wu, B. Y. Xia, C. Y. Xu and X. W. Lou, Hierarchical beta-Mo_2C nanotubes organized by ultrathin nanosheets as a highly efficient electrocatalyst for hydrogen production, *Angew. Chem., Int. Ed.*, 2015, **54**, 15395–15399.

38 X. F. Lu, L. Yu, J. Zhang and X. W. Lou, Ultrafine dual-phased carbide nanocrystals confinedin porous nitrogen-doped carbon dodecahedrons for efficient hydrogen evolution reaction, *Adv. Mater.*, 2019, **31**, 1900699.

39 A. A. Koverga, A. M. Gomez-Marin, L. Dorkis, E. Florez and E. A. Ticianelli, Role of transition metals on TM/Mo_2C composites: hydrogen evolution activity in mildly acidic and alkaline media, *ACS Appl. Mater. Interfaces*, 2020, **12**, 27150–27165.

40 J. J. Huang, J. Y. Wang, R. K. Xie, Z. H. Tian, G. L. Chai, Y. W. Zhang, F. L. Lai, G. J. He, C. T. Liu, T. X. Liu, P. R. Shearing and D. J. L. Brett, A universal pH range and a highly efficient Mo_2C-based electrocatalyst for the hydrogen evolution reaction, *J. Mater. Chem. A*, 2020, **8**, 19879–19886.

41 J. Wang, S. W. Li, J. Hu, S. Q. Niu, Y. Z. Li and P. Xu, Acid-directed morphology control of molybdenum carbide embedded in a nitrogen doped carbon matrix for enhanced electrocatalytic hydrogen evolution, *Inorg. Chem. Front.*, 2020, **7**, 3620–3626.

42 H. L. Lin, N. Liu, Z. P. Shi, Y. L. Guo, Y. Tang and Q. S. Gao, Cobalt-doping in molybdenum-carbide nanowires toward efficient electrocatalytic hydrogen evolution, *Adv. Funct. Mater.*, 2016, **26**, 5590–5598.